© Pol J Radiol 2025; 90: e582-e590
DOI: https://doi.org/10.5114/pjr/209215

Received: 27.05.2025
Accepted: 10.08.2025
Published: 02.12.2025

Polish Journal of Radiology

http://www.polradiol.com

Review paper

Quantification of liver iron overload among pediatric patients with magnetic resonance imaging: current state of the art

Gabriela Alicja Hryniewicz[1,A,B,D,E,F], Dominik Święton[1,A,D,E,F], Małgorzata Grzywińska[2,A,D,E,F], Kacper Marunowski[1,A,D,E], Maciej Piskunowicz[3,A,B,D,E]

[1]2nd Department of Radiology, Medical University of Gdansk, Poland
[2]Department of Neurophysiology, Neuropsychology and Neuroinformatics, Medical University of Gdansk, Poland
[3]1st Department of Radiology, Medical University of Gdansk, Poland

Abstract

Secondary iron overload in pediatric oncology patients is related to excessive iron accumulation in the liver, with subsequent cirrhosis and dangerous complications affecting numerous other organs. Liver iron concentration (LIC) correlates linearly with the total body iron stores; therefore, the quantification of hepatic iron is of major research interest. Although liver biopsy has been considered the gold standard for identifying iron overload, magnetic resonance imaging (MRI) is a non-invasive and highly accurate alternative method for the assessment of hemochromatosis. Our intention is to present a brief description of MRI-based procedures and a comparison of selected methods. Briefly, among the available methods, the liver-to-muscle signal intensity is accessible and easy to apply; however, it assumes that muscle is pathology-free, which may not always be true.

Transverse relaxometry is a valid method and allows for the identification of a low iron burden. However, this technique is unfortunately prone to motion artifacts and provides inconsistent results in cases of heavy iron overload.

Finally, quantitative susceptibility mapping (QSM) is a notable procedure considered to be of significant interest for the future. The exact correlation between QSM and LIC, as measured by liver biopsy has yet to be established.

Key words: MRI, pediatric oncology, signal intensity ratio, *T2* relaxometry, hepatic iron overload, quantitative susceptibility mapping.

Introduction

Iron is an essential component of numerous proteins involved in vital metabolic processes, such as hemoglobin and cytochromes [1]. However, when present in excess, iron can be highly toxic and lead to dangerous multi-organ complications. Since the body lacks natural mechanisms to excrete iron, any excess is first stored in the liver, which serves as the primary organ for iron storage. When iron accumulation becomes severe, the consequences appear in other organs, including the spleen, pancreas, bone marrow, heart, and endocrine glands.

Detecting iron overload in pediatric oncology poses a diagnostic challenge for clinicians due to the asymptomatic onset of hemochromatosis. Secondary hemochromatosis represents a significant clinical problem in hemato-oncologic patients, and requires close collaboration between oncologists and radiologists. Due to the dynamic development of radiology over the last two decades, numerous non-invasive methods for assessing iron overload have been introduced and examined.

Magnetic resonance imaging (MRI) is a universally accepted and favored method of evaluating liver iron overload. Despite various publications on MRI techniques,

Correspondence address:
Gabriela Alicja Hryniewicz, 2nd Department of Radiology, Medical University of Gdansk, 17 M. Smoluchowskiego St., 80-214 Gdansk, Poland,
e-mail: g.hryniewicz@gumed.edu.pl

Authors' contribution:
A Study design · **B** Data collection · **C** Statistical analysis · **D** Data interpretation · **E** Manuscript preparation · **F** Literature search · **G** Funds collection

there is still a lack of standardized quantification of liver iron concentration (LIC) using MRI in the pediatric population.

Magnetic resonance techniques for assessing tissue iron content can be categorized into two groups: signal intensity ratio (SIR) and relaxometry. Within these categories, several techniques have been identified, including methods that assess SIR based on *T2*-weighted (spin-echo) or *T2**-weighted (gradient-echo) sequences, relaxometry methods that measure absolute *T2*, relaxometry methods that measure absolute *T2**, and quantitative susceptibility mapping (QSM) [2-5]. Most of these techniques have been discussed before in relation to adult patients. In this article, we present a brief description of those methods, followed by a more detailed insight into the advantages and limitations of the presented techniques. Our goal is to explore the application of these techniques in a pediatric oncology setting while considering the limitations associated with imaging children. In this patient population, the duration of procedures and the use of anesthesia are critical factors. The most extensively studied group of patients with hemochromatosis consists of adolescents diagnosed with beta-thalassemia major. Evaluating pediatric oncology patients may require a different approach due to factors such as their higher water content compared to adult tissues. Further research in the population of pediatric oncology is much needed.

Relaxation theory

The assessment of iron accumulation in tissue relies on *T2*-relaxation shortening. Ferritin-bound iron affects MRI signal through the spin-spin relaxation mechanism, which impacts how signals are emitted from tissue during the examination. Hemosiderin iron creates magnetic field inhomogeneities that lead to spin dephasing. These properties are used to estimate tissue iron levels. Interactions between these proteins and water molecules cause increased *T2* relaxation [4]. The difference in solubility and intracellular distribution between ferritin iron (soluble, evenly spread out) and hemosiderin iron (insoluble, grouped in irregular micron-sized clusters with separations of 10-30 μm) [6] leads to diverse effects on MRI signal deterioration. Ferritin iron primarily influences MRI signal decay through molecular spin–spin relaxation mechanisms, whereas hemosiderin clusters predominantly create magnetic field inconsistencies that result in spin dephasing [7,8]. Current MRI techniques used to estimate tissue iron levels aim to measure the total iron deposition (ferritin + hemosiderin) by analyzing SIRs or relaxation rates [9,10] via equations such as $R2 = 1/T2$ and $T2^* = 1/T2^*$.

SIR

The SIR method is based on the comparison of the signal from the paraspinal muscle and liver obtained from multiple gradient-echo sequences (GREs). Both SIR methods – one proposed by Gandon, and the other by Alústiza – have been verified at 1.5 *T*.

In 2004, subsequent adjustments to the technique were introduced by Gandon *et al.* [4], who proposed dividing the signal intensity of the specific organ by the signal intensity of a reference tissue (fat or muscle) or noise. Signal-intensity assessments are conducted in five separate breath-hold GREs; this approach allows for constant *TR* (repetition time) but operates on various angles from 20° to 90° to adjust *T1* and *T2* weighting with echo times ranging from 4 to 21 ms.

Castiella *et al.* [11] proposed a method that employs only two echo times (4 and 14 ms) and a different mathematical formula to estimate the LIC. Studies show that the model of the Spanish Society of Abdominal Imaging produces results that are more closely associated with *R2** and LIC values obtained from liver biopsies [12].

The suggested procedure for SIR analysis involves placing three regions of interest (ROIs), including one in the right lobe of the liver and two in the left and right paraspinal muscles. This can result in divergent liver/muscle SIRs among all five sequences [13].

For SIR calculation, different reference tissues have been considered; however, the paraspinal muscles have emerged as the preferred option due to their optimal balance of sensitivity and minimal intersite variability [4,12,14]. However, in patients with sarcopenia or myosteatosis, muscle tissue may be a source of additional unpredictability.

In the case of larger organs such as the liver, spleen, and pancreas, multiple ROIs are used and placed in regions lacking vascular structures and motion artifacts [4,5,15,16].

The SIR method relies on detecting a decrease in signal intensity due to *T2** shortening in iron overload-affected organs compared to a reference tissue that is assumed to be free of iron accumulation. In this comparison, the signal intensity of healthy tissue (without iron overload) should consistently surpass that of the paraspinal muscles [13].

The biggest drawback of this method is the lack of reliability with iron level > 19.5 mg/g dry weight. Due to the chemical shift caused by iron-bound proteins, the signal from the liver in cases of heavy iron overload may be completely lost [17].

Gandon *et al.* [4] did not find any significant relationship between liver steatosis and the reliability of LIC measurements. They highlighted that fatty liver primarily affects signals from *T1*-weighted images. Despite these findings, the effect of steatosis and fat saturation on the assessment of iron overload still requires further research [18]. Standardization of parameters during the procedure could improve the validity of the results.

T2 relaxometry method

Evaluating the *T2* relaxation time (transverse relaxation) reveals the loss of coherence between individual protons

following a radiofrequency pulse. The paramagnetic characteristics of iron reduce the *T2* relaxation time, allowing for an evaluation of hepatic iron overload [19]. This technique typically requires five echo times (6, 9, 12, 15, and 18 ms) and a repetition time of 2500 ms [20].

The "speed-up" of *T2* relaxation is proportional to the degree of iron burden in the examined tissue, resulting in a decay of signal intensity in the liver [21]. The transverse magnetization decay curve illustrates the relationship between the transverse magnetization over time following deactivation of the radiofrequency pulse. Relaxometry is assessed using the voxel technique, which allows for reliable tissue evaluation and reduces the risk of operator-dependent error. During the calculation of *T2* relaxation time, a single voxel is meticulously positioned within the liver, clear of significant vessels, large bile ducts, and lesions. It is typically placed in the posterolateral portion of the right lobe; however, the final position depends on the protocol and the presence of artifacts. The signal intensity from the single voxel is then plotted against the echo times. The following exponential decay function is then fitted to these data points:

$$S(TE) = S_0 \, exp\left(-\frac{TE}{T2}\right)$$

The signal intensity (S) at each echo time (TE) follows the free induction decay (FID) curve, which is influenced by *T2**. Here, S_0 represents the initial height of the FID curve. *T2** is a combined relaxation time that incorporates *T2*, the effects of main field inhomogeneities, tissue susceptibility, and proton diffusion [22].

The transverse relaxation process within an iron-overloaded liver is considered at least biexponential by nature. Exponential *R2* image analysis involves estimating the initial signal from protons within a specific ROI. This estimation takes into account the strength of the radiofrequency field. Creating a map of how dense the proton spins are requires considering a material that surrounds the analyzed area with a high density of spins and a long relaxation time (*T2*) [22,23]. Based on this, the map of *T2* relaxation for the liver can be generated.

An analytical model was developed to create the standardization curve linking liver *R2* values with LIC values obtained from biopsy [24]. This involved fitting curves to the data using non-linear regression algorithms. This calibration curve was obtained from phantoms or known standards. The calibration relationship derives the LIC from the *T2* values. Lower *T2* values indicate higher iron concentrations.

T2* relaxometry method

Unevenly distributed iron deposits behave like tiny bar magnets, creating small-scale magnetic field inhomogeneities. These irregularities cause protons within a voxel to spin at varying frequencies, leading to *T2** relaxation, which is influenced by these variations in the main magnetic field.

This method is used to assess *T2** or by employing multiple gradient-echo sequences with different *TE* values [10]. The aim is to speed up data acquisition to improve sensitivity and eliminate artifacts from respiration or cardiac motion. In calculating *R2** values, the signal decay curve is commonly modeled using an exponential function, as follows:

$$S(TE) = S_0^* \, exp\left(-\frac{TE}{T2^*}\right) + C$$

where S is the signal intensity, TE is the echo time, and S_0 represents a constant signal intensity [10]. Breath-hold sequences eliminate interslice variability caused by differences resulting from patient movements [25]. This technique has been mainly used to assess myocardial overload with cardiac gating [26-28]. The technique is not free of limitations, which include measurement variability caused by factors such as noise disruption, associated liver fat, or magnetic field dissimilarities.

QSM

QSM is a robust, non-invasive MRI method that measures magnetic susceptibility [29]. This approach may be a new technique for examining iron overload, as it demonstrates a good correlation with LIC. The major advantage of QSM is that it allows for the assessment of hepatic iron without interference from conditions such as fibrosis and fat. QSM quantifies the spatial distribution of magnetic susceptibility (χ) generated by the magnetic properties within the tissues [29]. The magnetic susceptibility distribution consists of local and background susceptibility. Local susceptibility represents the susceptibility disruption within the tissue of interest, usually originating from ferritin or hemosiderin. Two or more echoes can assess the local magnetic field. Later, this information can be used to calculate the magnetic field distribution relative to the underlying susceptibility distribution [29]. All images are captured within a single breath-hold. This requirement makes applying QSM challenging in a pediatric oncology setting, especially for young children. The image process uses short echo times and minimal echo spacing to capture the rapidly weakening signal, especially in cases of significant hemosiderosis [29].

The magnetic susceptibility disruption (χ) can be separated into two components: local (χ_L) – within spatial ROIs (e.g. tissue); and background (χ_B) – outside of the ROI. As a result, each spatial point within the susceptibility distribution corresponds to either χ_L or χ_B, but not to both simultaneously. There is a mathematical correlation between the susceptibility distribution and the shift in resonance frequency induced by inhomogeneities in the B_0 field [30]. The estimation of the B_0 field map is achieved through chemical shift-encoded reconstruction, which

incorporates models of water and different fat peaks in the spectrum. During the reconstruction process, spectral modeling corrects the B_0 field map for the presence of fat [29]. There is a linear relationship between liver iron concentration and magnetic susceptibility, which facilitates reliable quantification of liver iron using QSM. After creating the quantitative susceptibility map, a local relative susceptibility value (ΔB_0), in parts per million (ppm), can be derived from a specific ROI. This value can then be compared with the amount of hepatic iron [29].

The prospect of using QSM for examining the pancreas seems very promising. Kemp *et al.* [31] emphasize its potential to be a new, highly sensitive tool for diagnosing and monitoring pancreas-related diseases, such as metabolic syndrome and endocrine dysfunction.

Comparison of MRI methodologies

The SIR method is generally considered the easiest method to apply across various vendors and platforms. According to guidelines from the European Society of Gastrointestinal and Abdominal Radiology (ESGAR) and the Society of Abdominal Radiology, SIR is considered a practical alternative when high-quality phased-array coils or relaxometry techniques are unavailable. This approach, however, has certain limitations. It shows reduced sensitivity in detecting severe siderosis in tissues where transverse relaxation occurs much faster than the *TE* [14]. Different investigators have proposed modifications to this method to improve its accuracy in the evaluation of severe siderosis [19]. Still, the SIR method is not suited to measure LIC values above 350 μmol Fe/g; in these instances, it simply categorizes the iron overload as "very high." Although patients with such high iron levels clearly require treatment, the method's inability to distinguish the full range of clinically significant LIC values is a drawback.

The SIR method also relies on the assumption that muscle is free of pathology. This assumption may be false in pediatric oncology patients, who are at high risk of sarcopenia or myosteatosis [31,32]. Relying on a reference tissue (muscle) adds extra variability, especially at low-to-moderate LIC levels and in patients with reduced muscle mass.

Another limitation of the SIR method pertains to the recommendation to use only the body coil and avoid surface coils, particularly those integrated into the patient's bed. This precaution prevents signal gradients between the surface and depth. Failure to follow this guideline can result in a decrease in signal-to-noise efficiency. Even though the method involves "in-phase" echoes, it is essential to note that it does not address fat content, which may introduce notable bias [33]. When fat and water are present within the same pixel, opposed-phase GRE images present a relative loss in signal intensity [4].

Numerous studies have demonstrated a strong correlation between both T2 and T2* values and LIC as measured in liver biopsy for evaluating liver iron overload. However, these techniques come with certain challenges; their measurements are influenced by the MRI sequence parameters and the image-analysis method, and there is no universal agreement on which index (*R2* or *R2**) is optimal for measuring LIC. *T2** calculations are sensitive to low iron content, but tend to be less accurate in cases of high iron overload. Another limitation is the requirement for a large number of echoes to sample the entire exponential decay of the transverse magnetization and minimize the uncertainty in the measured *T2* result [34]. Another challenge is the selection of the calibration curve and its impact on the transferability of *R2** measurements, regardless of the scanner type. To our knowledge, several studies have investigated calibration curves for MRI-based liver iron quantification. Henninger *et al.* [35] found a good correlation between the curves designed by his team and those of three other researchers – Wood [36], Hankins [37], and Garbowski [24,38]. A more standardized approach to MRI-based iron overload assessment is urgently needed [39].

The *R2* method described by St. Pierre *et al.* requires an average data-acquisition time of 20 min, in contrast with the few minutes needed for implementing single breath-hold techniques [40]. However, examination times vary between different institutions and countries. Twenty minutes is a relatively short procedure. The time a patient spends inside the scanner is important, especially considering the unique needs of pediatric patients and procedural costs.

QSM has been a useful tool for the evaluation of brain iron levels. It has promising clinical applications, as it provides an opportunity to directly measure liver iron concentration based on MR susceptibility. However, the application of QSM in the abdomen faces additional challenges such as respiratory motion artifacts, the presence of fat, and rapid signal decay in cases of heavy iron overload. When LIC values are high, both the *R2** estimates and the B_0 field map are unreliable, which subsequently reduces the reliability of susceptibility map estimation. Background field removal and dipole inversion impose further difficulties [29]. Studies examining the accuracy of QSM have shown significant discrepancies, the causes of which remain unclear. Sharma *et al.* [30] attributed these discrepancies to the large spatial resolution, including slice thickness above 8 mm. In their study, large slices were necessary to obtain complete 3D coverage of the liver in a single breath-hold. This example highlights the need for standardized protocols and extensive research in this area.

QSM still has the potential to become an imaging biomarker of liver iron burden. The major advantage of quantifying susceptibility lies in using fundamental material properties (including iron and liver tissue), in contrast with experimental relaxation parameters (e.g., *R2* and *R2**), which may be disrupted by other factors [30].

All of the presented methods face certain challenges and significant limitations. Continued research is necessary to identify optimal imaging biomarkers that allow

for quick, reliable, and cost-effective evaluations of iron overload in the pediatric oncology setting.

Table 1 presents a brief comparison of previously discussed methods of evaluating iron overload. No ideal technique for assessing hemochromatosis has been created; different methods are accurate for different organs.

Summary

Iron overload is a serious condition that can lead to multi-organ complications in the pediatric oncology population. MRI offers highly effective tools for the non-invasive assessment of iron overload, allowing for early detection and monitoring. However, various confounding factors, such as image noise and intrahepatic fat, must be considered in MRI-based LIC assessment. Three primary MRI techniques – SIR, *R2*, and *R2**– have been developed and validated. Based on the available literature, confounder-corrected *R2**-based LIC appears to be the most practical method, offering the strongest evidence for accurate and reproducible quantification. These methods are commercially available for both 1.5-*T* and 3-*T* MRI scanners and are recommended as first-line approaches for iron quantification when available. SIR and *R2*-based LIC quantification are also reliable alternatives, with moderate-to-high levels of evidence supporting their use [41].

The ability to accurately estimate iron overload is crucial for treatment monitoring, including avoiding over- and undertreatment, maintaining safe levels of iron, and reducing the risk of dangerous long-term complications. It is necessary to standardize non-invasive measurements of LIC so that clear inferences can be drawn about body iron levels associated with hepatic and extra-hepatic complications of iron overload. Examples of proposed references are presented in Table 2 [4,12,18,28,42].

In the adult population, both *T2**-weighted imaging and the SIR method are commonly used; however, only *T2** is considered the method of choice for assessing cardiac iron overload due to its functional mobility. QSM is increasingly used for the assessment of iron overload in the pancreas and spleen. In the pediatric population, the most common and well-characterized cause of secondary iron overload is frequent blood transfusions. So far, there is a lack of literature comparing iron overload resulting from chemotherapy to that caused by blood transfusions. For the pediatric population, the *T2** technique remains the gold standard for evaluating hepatic and cardiac iron overload, while SIR is considered insufficiently accurate [38].

The lack of reference value ranges significantly limits the use of MRI in the pediatric population, regardless of the method used to assess iron overload. We conducted a thorough search and analyzed nine studies, focusing on accepted reference values across various centers. To date, only two studies – one by Wood and the other by Berdoukas – have examined pediatric and adolescent populations. Wood *et al.* [27] focused solely on transfusion-dependent iron overload, measuring *T2* and studying correlations with clinical findings such as tachycardia and depressed ejection fraction. Secondary iron overload is usually detected in adulthood during the diagnostic process for chronic diseases such as heart failure; how-

Table 1. Comparison of methods of evaluating iron overload.

Methods	Advantages	Limitations
Signal intensity ratio	Simplest method Adaptable (to various imaging systems) Cost-free post-processing and calculation for 1.0-*T*, 1.5-*T*, and 3.0-*T* imaging	Unreliable for severe iron overload > 19.5 mg/g dry weight Assumption that reference tissue is free of abnormalities
T2 relaxometry	Correlates strongly with results of liver biopsy More comfortable for patients – free breathing technique	Respiratory motion artefacts Inconsistent with higher iron overload levels > 20 mg/g dry weight Fat saturation is not incorporated Extra expenses and processing delays Extended data acquisition duration
*T2** relaxometry	Reliable for liver iron overload Single or multiple breath hold technique – reduced motion artefacts Simultaneous analysis of liver steatosis and iron overload Compatible with both 1.5-*T* and 3.0-*T* imaging	Post-processing algorithms are exclusively available for purchase and might not be universally accessible
Quantitative susceptibility mapping (QSM)	The most sensitive MRI method for identifying iron deposits Capability to correct fat presence All acquisitions in a single breath Susceptibility values can be compared across different field strengths	Utilized mainly for research purposes and is not standardized The direct relationship between quantitative susceptibility mapping values and liver iron content has not been definitively established

Table 2. MRI-based reference and threshold values for iron quantification across organs

Author (year)	Age of participants	Number of participants	MRI technique	Organ	Cause of iron overload	Reference/threshold values (mg/g dry weight, *T2**ms, *R2** Hz)	Additional information
Gandon (2004)	Unknown	174	SIR	Liver	Hepatic iron overload or chronic hepatitis C	< 36 µmol/g (norm) > 60 µmol/g (overload)	Correlation with biopsy
Anderson (2001)	13-41	106	*T2** Relaxometry	Heart, spleen	Transfusions (beta-thalassemia major)	Liver *T2** 52 ± 16 ms (norm) Liver *T2** < 20 ms (overload) Splenic *T2** 56 ± 22 ms (norm) remarkable variations	Correlation between myocardial T2* and liver T2*
Au (2008)	12-47	72	*T2** Relaxometry	Pancreas	Transfusions (beta-thalassemia major)	*T2** 21.3-53 ms (norm) *T2** < 21 ms (overload)	Correlation with myocardial *T2** and metabolic data
Schwenzer (2008)	20-70	129	*T2** Relaxometry	Liver, spleen	No history of iron overload	Liver *T2** 13.6-45.9 ms (norm) Spleen *T2** 14.4-113.6 ms (norm)	Correlation with metabolic and anthropometric data
Schwenzer (2008)	20-70	61	*T2** Relaxometry	Pancreas	No history of iron overload	*T2** values 25.9-64.8 ms (norm) *T2** < 21 ms (overload)	Correlation with metabolic and anthropometric data
Maris (2007)	13-40	69	*T2** Relaxometry	Liver	Transfusions (beta-thalassemia major)	Liver *T2** 24.2 ± 3.0 ms (norm) *T2** Liver/muscle 0.192-0.13 ms (overload)	Correlation between myocardial *T2** and liver *T2**
Berdoukas (2013)	0-10	125	*T2** Relaxometry	Pancreas	Transfusions (sickle cell anemia, beta-thalassemia major, Diamond-Blackfan anemia)	Pancreatic *R2** < 27 Hz (norm) Pancreatic *R2** > 100 Hz (overload)	Correlation with diabetes mellitus
Noetzli (2011)	10-49	59	*T2** Relaxometry	Pancreas, heart	Transfusions (beta-thalassemia major)	No normal range reported Pancreas *R2** > 100 Hz (overload) Cardiac *R2** > 50 Hz (overload)	Correlation with diabetes mellitus
Wood (2010)	7-26	36	*T2** Relaxometry	Spleen	Transfusions (sickle cell anemia, beta-thalassemia major)	Cardiac *T2** 30-40 ms (normal range); Cardiac *T2**< 25 ms (overload)	Less frequently assessed than the liver

ever, the age at which it first occurs remains unknown. Berdoukas *et al.* [43] attempted to establish the dynamics of iron overload in the pancreas, liver, and heart in different diseases (sickle cell anemia, beta-thalassemia major, Diamond-Blackfan anemia). They also reported having similar data for patients receiving chemotherapy. However, to date, there are no similar publications regarding pediatric oncology patients receiving chemotherapy. This highlights the need for careful tissue iron monitoring to establish iron loading patterns and to develop optimized methods for pediatric oncology patients.

Improving the accessibility of MRI methods and validating their efficacy in pediatric oncology settings is crucial. Long-term follow-up of pediatric oncology patients using MRI techniques will significantly improve their quality of life and reduce the risk of premature mortality.

Based on the available literature, confounder-corrected *R2**-based LIC appears to be the most practical method, offering the strongest evidence for accurate and reproducible quantification. Figures 1-3 present the use of *R2* analysis for automatic liver iron quantification.

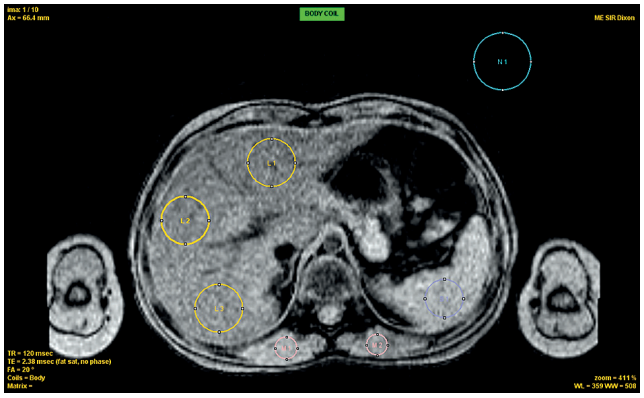

Figure 1. ROI placement for *R2** analysis Axial ME-GRE image showing ROIs for liver (L1-L3, yellow), spleen (S1, blue), muscle (M1-M2, red), and background noise (N1, cyan). ROIs were selected to avoid vessels and organ boundaries. Acquisition: $TR = 120$ ms, $TE = 2.38$ ms, $FA = 20°$

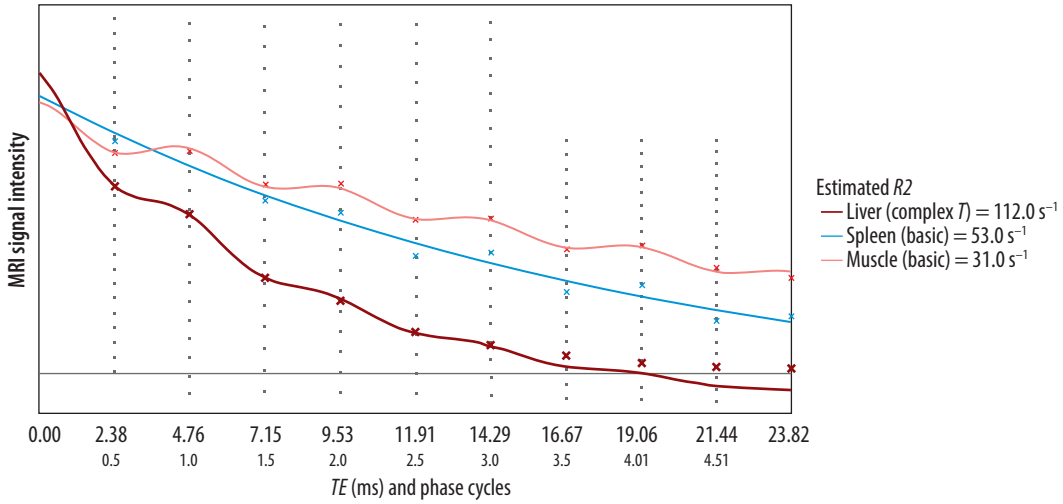

Figure 2. Signal decay curves and *R2** fitting. Signal intensity decay as a function of echo time (*TE*) for liver (red), spleen (blue), and muscle (pink). Liver shows rapid signal loss, indicating elevated *R2** (112 s^{-1}). Spleen and muscle show slower decay (53 and 31 s^{-1}, respectively). Noise level is indicated by the horizontal line (62.6). Curves are fitted using exponential models

Hepatic MRI with iron and fat quantification

Patient: Mr. HEMO , born on April 13, 2025 (007Y years)

carried out on November 30, 0002

INDICATION:

Evaluation of hepatic iron and fat concentration.

PROTOCOL

Examination carried out on an MRI machine 1.5 Tesla MAGNETOM Sola (Siemens Healthineers).

RESULTS

Liver:
The signal decay is increased on the longest echoes. The R2* is estimated at 99 s-1 using a complex exponential decay. The **R2*/B0** index is **66** (N<50). The conversion formula proposed by Gandon, providing an intermediate value between that proposed by Garbowski at 1.5T and d'Assignies at 3T, comparable whatever the device, estimates the iron concentration at **60 µmol/g**in dry weight (N<36 µmol/g).
Presence of a slight lowering of the signal on anti-phase echoes. The fat fraction estimated by complex signal modeling taking into account the main peaks of fat is **6.7 %**. The steatosis score corresponding to the percentage of hepatocytes containing fat vacuoles is between 13 and 20% (two to three times the fat fraction).

Spleen:
The signal decays normally on in-phase echoes. The R2* is estimated at 53 s-1 using a simple exponential decay. The conversion formula proposed by Gandon estimates the iron concentration at **32 µmol/g**in dry weight. However this value is purely indicative because there is no correlation validation published in the literature.

Figure 3. Automated liver iron and fat quantification report. R2* in the liver is 99 s^{-1}, corresponding to an iron concentration of 60 µmol/g dry weight. Fat fraction is estimated at 6.7%, consistent with mild steatosis (13-20% of hepatocytes affected). Spleen R2* is 53 s^{-1} with an indicative iron level of 32 µmol/g

Disclosures

1. Institutional review board statement: Not applicable.
2. Assistance with the article: None.
3. Financial support and sponsorship: None.
4. Conflicts of interest: None.

References

1. Siah CW, Ombiga J, Adams LA, Trinder D, Olynyk JK. Normal iron metabolism and the pathophysiology of iron overload disorders. Clin Biochem Rev 2006; 27: 5-16.
2. Kaltwasser JP, Gottschalk R, Schalk KP, Hartl W. Non-invasive quantitation of liver iron-overload by magnetic resonance imaging. Br J Haematol 1990; 74: 360-363. DOI: 10.1111/J.1365-2141.1990.TB02596.X
3. Gossuin Y, Muller RN, Gillis P. Relaxation induced by ferritin: a better understanding for an improved MRI iron quantification. NMR Biomed 2004; 17: 427-432. DOI: 10.1002/NBM.903.
4. Gandon Y, Olivié D, Guyader D, Aubé C, Oberti F, Sebille V, et al. Non-invasive assessment of hepatic iron stores by MRI. Lancet 2004; 363: 357-362. DOI: 10.1016/S0140-6736(04)15436-6.
5. Martin DR. Liver-iron assay by MRI. Lancet 2004; 363: 341-342. DOI: 10.1016/S0140-6736(04)15471-8.
6. Ghugre NR, Coates TD, Nelson MD, Wood JC. Mechanisms of tissue-iron relaxivity: nuclear magnetic resonance studies of human liver biopsy specimens. Magn Reson Med 2005; 54: 1185-1193. DOI: 10.1002/MRM.20697.
7. Gossuin Y, Roch A, Muller RN, Gillis P, Lo Bue F. Anomalous nuclear magnetic relaxation of aqueous solutions of ferritin: an unprecedented first-order mechanism. Magn Reson Med 2002; 48: 959-964. DOI: 10.1002/MRM.10316.
8. St Pierre TG, Clark PR, Chua-Anusorn W. Single spin-echo proton transverse relaxometry of iron-loaded liver. NMR Biomed 2004; 17: 446-458. DOI: 10.1002/NBM.905.
9. Gattermann N, Muckenthaler MU, Kulozik AE, Metzgeroth G, Hastka J. The Evaluation of iron deficiency and iron overload. Dtsch Arztebl Int 2021; 118: 847-856. DOI: 10.3238/ARZTEBL.M2021.0290.
10. Argyropoulou MI, Astrakas L. MRI evaluation of tissue iron burden in patients with beta-thalassaemia major. Pediatr Radiol 2007; 37: 1191-1200. DOI: 10.1007/S00247-007-0567-1.
11. Castiella A, Alústiza JM, Emparanza JI, Zapata EM, Costero B, Díez MI. Liver iron concentration quantification by MRI: are recommended protocols accurate enough for clinical practice? Eur Radiol 2011; 21: 137-141. DOI: 10.1007/S00330-010-1899-Z.
12. Henninger B, Alustiza J, Garbowski M, Gandon Y. Practical guide to quantification of hepatic iron with MRI. Eur Radiol 2024; 30: 383-393. DOI: 10.1007/S00330-019-06380-9.
13. Hernando D, Levin YS, Sirlin CB, Reeder SB. Quantification of liver iron with MRI: state of the art and remaining challenges. J Magn Reson Imaging 2014; 40: 1003-1021. DOI: 10.1002/JMRI.24584.
14. Fenzi A, Bortolazzi M, Marzola P. Comparison between signal-to-noise ratio, liver-to-muscle ratio, and 1/T2 for the noninvasive assessment of liver iron content by MRI. J Magn Reson Imaging 2003; 17: 589-592. DOI: 10.1002/JMRI.10306.
15. Ernst O, Sergent G, Bonvarlet P, Canva-Delcambre V, Paris JC, L'Herminé C. Hepatic iron overload: diagnosis and quantification with MR imaging. AJR Am J Roentgenol 1997; 168: 1205-1208. DOI: 10.2214/ajr.168.5.9129412.
16. Rose C, Vandevenne P, Bourgeois E, Cambier N, Ernst O. Liver iron content assessment by routine and simple magnetic resonance imaging procedure in highly transfused patients. Eur J Haematol 2006; 77: 145-149. DOI: 10.1111/j.0902-4441.2006.t01-1-EJH2571.x.
17. Queiroz-Andrade M, Blasbalg R, Ortega CD, Rodstein MAM, Baroni RH, Rocha MS, et al. MR imaging findings of iron overload. Radiographics 2009; 29: 1575-1589. DOI: 10.1148/RG.296095511.
18. Sirlin CB, Reeder SB. Magnetic resonance imaging quantification of liver iron. Magn Reson Imaging Clin N Am 2010; 18: 359-381. DOI: 10.1016/J.MRIC.2010.08.014.
19. Alústiza Echeverría JM, Castiella A, Emparanza JI. Quantification of iron concentration in the liver by MRI. Insights Imaging 2012; 3: 173-180. DOI: 10.1007/s10334-012-0324-4.
20. St. Pierre TG, Clark PR, Chua-Anusorn W. Measurement and mapping of liver iron concentrations using magnetic resonance imaging. Ann N Y Acad Sci 2005; 1054: 379-385. DOI: 10.1196/annals.1345.046.
21. Jensen JH, Chandra R. Theory of nonexponential NMR signal decay in liver with iron overload or superparamagnetic iron oxide particles. Magn Reson Med 2002; 47: 1131-1138. DOI: 10.1002/MRM.10170.
22. McRobbie DW, Moore EA, Graves MJ, Prince MR. Getting in tune: resonance and relaxation. In: MRI from picture to proton. Cambridge: Cambridge University Press; 2006. p. 137-166.
23. Clark PR, Chua-Anusorn W, St. Pierre TG. Bi-exponential proton transverse relaxation rate (R2) image analysis using RF field intensity-weighted spin density projection: potential for R2 measurement of iron-loaded liver. Magn Reson Imaging 2003; 21: 519-530. DOI: 10.1016/S0730-725X(03)00080-8.
24. Garbowski MW, Carpenter JP, Smith G, Roughton M, Alam MH, He T, et al. Biopsy-based calibration of T2* magnetic resonance for estimation of liver iron concentration and comparison with R2 Ferriscan. J Cardiovasc Magn Reson 2014; 16: 40. DOI: 10.1186/1532-429X-16-40.
25. Schwenzer NF, MacHann J, Haap MM, Martirosian P, Schraml C, Liebig G, et al. T2* relaxometry in liver, pancreas, and spleen in a healthy cohort of one hundred twenty-nine subjects-correlation with age, gender, and serum ferritin. Invest Radiol 2008; 43: 854-860. DOI: 10.1097/RLI.0B013E3181862413.
26. Jensen PD, Jensen FT, Christensen T, Eiskjær H, Baandrup U, Nielsen JL. Evaluation of myocardial iron by magnetic resonance imaging during iron chelation therapy with deferrioxamine: indication of close relation between myocardial iron

content and chelatable iron pool. Blood 2003; 101: 4632-4639. DOI: 10.1182/BLOOD-2002-09-2754.
27. Wood JC, Tyszka JM, Carson S, Nelson MD, Coates TD. Myocardial iron loading in transfusion-dependent thalassemia and sickle cell disease. Blood 2004; 103: 1934-1936. DOI: 10.1182/BLOOD-2003-06-1919.
28. Anderson LJ, Holden S, Davis B, Prescott E, Charrier CC, Bunce NH, et al. Cardiovascular T2-star (T2*) magnetic resonance for the early diagnosis of myocardial iron overload. Eur Heart J 2001; 22: 2171-2179. DOI: 10.1053/EUHJ.2001.2822.
29. Labranche R, Gilbert G, Cerny M, Vu KN, Soulières D, Olivié D, et al. Liver iron quantification with MR imaging: a primer for radiologists. Radiographics 2018; 38: 392–412. DOI: 10.1148/RG.2018170079.
30. Sharma SD, Hernando D, Horng DE, Reeder SB. Quantitative susceptibility mapping in the abdomen as an imaging biomarker of hepatic iron overload. Magn Reson Med 2015; 74: 673-683. DOI: 10.1002/MRM.25448.
31. Kemp JM, Ghosh A, Dillman JR, Krishnasarma R, Manhard MK, Tipirneni-Sajja A, et al. Practical approach to quantitative liver and pancreas MRI in children. Pediatr Radiol 2025; 55: 36-57. DOI: 10.1007/S00247-024-06133-X.
32. Mueske NM, Mittelman SD, Wren TAL, Gilsanz V, Orgel E. Myosteatosis in adolescents and young adults treated for acute lymphoblastic leukemia. Leuk Lymphoma 2019; 60: 3146-3153. DOI: 10.1080/10428194.2019.1623889.
33. Ritz A, Lurz E, Berger M. Sarcopenia in children with solid organ tumors: an instrumental era. Cells 2022; 11: 1278. DOI: 10.3390/CELLS11081278.
34. Hernando D, Kühn JP, Mensel B, Völzke H, Puls R, Hosten N, et al. R2* estimation using 'in-phase' echoes in the presence of fat: the effects of complex spectrum of fat. J Magn Reson Imaging 2013; 37: 717-726. DOI: 10.1002/JMRI.23851.
35. Henninger B, Zoller H, Rauch S, Finkenstedt A, Schocke M, Jaschke W, et al. R2* relaxometry for the quantification of hepatic iron overload: biopsy-based calibration and comparison with the literature. Rofo 2015; 187: 472-479. DOI: 10.1055/S-0034-1399318
36. Wood JC. Use of magnetic resonance imaging to monitor iron overload. Hematol Oncol Clin North Am 2014; 28: 747-764. DOI: 10.1016/J.HOC.2014.04.002.
37. Hankins JS, McCarville MB, Loeffler RB, Smeltzer MP, Onciu M, Hoffer FA, et al. R2* magnetic resonance imaging of the liver in patients with iron overload. Blood 2009; 11: 4853-4855. DOI: 10.1182/BLOOD-2008-12-191643.
38. Alústiza JM, Emparanza JI, Castiella A, Casado A, Garrido A, Aldazábal P, et al. Measurement of liver iron concentration by MRI is reproducible. Biomed Res Int 2015; 2015: 294024. DOI: 10.1155/2015/294024.
39. Wood JC, Enriquez C, Ghugre N, Tyzka JM, Carson S, Nelson MD, et al. MRI R2 and R2* mapping accurately estimates hepatic iron concentration in transfusion-dependent thalassemia and sickle cell disease patients. Blood 2005; 106: 1460-1465. DOI: 10.1182/BLOOD-2004-10-3982.
40. St. Pierre TG, Clark PR, Chua-Anusorn W, Fleming AJ, Jeffrey GP, Olynyk JK, et al. Noninvasive measurement and imaging of liver iron concentrations using proton magnetic resonance. Blood 2005; 105: 855-861. DOI: 10.1182/BLOOD-2004-01-0177.
41. Sharma SD, Fischer R, Schoennagel BP, Nielsen P, Kooijman H, Yamamura J, et al. MRI-based quantitative susceptibility mapping (QSM) and R2* mapping of liver iron overload: comparison with SQUID-based biomagnetic liver susceptometry. Magn Reson Med 2017; 78: 264-270. DOI: 10.1002/MRM.26358.
42. Reeder SB, Yokoo T, França M, Hernando D, Alberich-Bayarri Á, Alústiza JM, et al. Quantification of liver iron overload with MRI: Review and guidelines from the ESGAR and SAR. Radiology 2023; 307: e221856. DOI: 10.1148/RADIOL.221856.
43. Berdoukas V, Nord A, Carson S, Puliyel M, Hofstra T, Wood J, Coates TD. Tissue iron evaluation in chronically transfused children shows significant levels of iron loading at a very young age. Am J Hematol 2013; 88: E283-E285. DOI: 10.1002/ajh.23543.